J. Fluid Mech., page 1 of 11. © Cambridge University Press 2011
doi:10.1017/jfm.2011.396

Evolution of the ejecta sheet from the impact of a drop with a deep pool

L. V. Zhang[1], J. Toole[1]‡, K. Fezzaa[2] and R. D. Deegan[1]†

[1] Department of Physics, and Center for the Study of Complex Systems, University of Michigan, Ann Arbor, MI 48109, USA

[2] X-Ray Science Division, Argonne National Laboratory, Argonne, IL 60439, USA

(Received 5 August 2011; revised 7 September 2011; accepted 13 September 2011)

We used optical and X-ray imaging to observe the formation of jets from the impact of a single drop with a deep layer of the same liquid. For high Reynolds number there are two distinct jets: the thin, fast and early-emerging ejecta; and the slow, thick and late-emerging lamella. For low Reynolds number the two jets merge into a single continuous jet, the structure of which is determined by the distinct contributions of the lamella and the ejecta. We measured the emergence time, position and speed of the ejecta sheet, and find that these scale as power laws with the impact speed and the viscosity. We identified the origin of secondary droplets with the breakup of the lamella and the ejecta jets, and show that the size of the droplets is not a good indicator of their origin.

Key words: breakup/coalescence, drops

1. Introduction

Splashing from the impact of a liquid drop with a solid or liquid surface occurs in a wide range of practical applications and natural phenomena: pesticide spraying (Spillman 1984), fuel injection systems (Reitz & Rutland 1995), cooling (Pasandideh-Fard *et al.* 2001), the transfer of gases across the air–sea interface (Wanninkhof *et al.* 2009) and the dispersal of biological agents (see Butterworth & McCartney 1991). The morphology of splashes and in particular the production mechanism of secondary droplets are not yet fully understood (for a recent review see Yarin 2006). Modelling difficulties arise from the nonlinearities, the broad range of length and time scales, the change of topology, and the uncertainty in the physics of the initial moments of impact when various poorly characterized effects are at play, such as bubble entrainment, compressibility of the surrounding gas, and singular pressures and curvatures. The situation with experiments is equally unsettled because of the vast parameter space (Rein 1993; Rioboo, Marengo & Tropea 2002; Rioboo *et al.* 2003; Cossali *et al.* 2004), the bewildering array of morphologies (Deegan, Brunet & Eggers 2008), and the technology challenging fast speeds and small scales of splashing.

† Email address for correspondence: rddeegan@umich.edu
‡ Present address: Engineering Systems Division, MIT, Cambridge, MA 02139, USA

The conventional picture of splashing from a wet impact event dates back to Worthington (1882). An axially symmetric sheet-like jet, the *lamella*, propagates outwards from the impact site; its leading edge develops corrugations, which grow, sharpen into cylindrical jets and pinch off to form a halo of secondary droplets. Weiss & Yarin (1999) showed that there exists a second jet, the *ejecta sheet*, which precedes the lamella. Using a boundary integral method to integrate the inviscid equations of motion, they found that, for sufficiently energetic impacts, the ejecta sheet emerges horizontally from the neck between the drop and the substrate fluid. The ejecta was subsequently observed experimentally by Thoroddsen (2002) and shown analytically by Howison *et al.* (2005).

One of our goals was to dispel the ambiguity that exists in the literature concerning the identity of the ejecta versus the lamella. Weiss & Yarin's (1999) ejecta reattached to the surrounding fluid or pinched off into a torus soon after forming. The fate of the ejecta in Thoroddsen (2002) is not explicitly stated, except in those cases where it was shown to disintegrate. The boundary integral method calculations of Davidson (2002) show no pinchoff but multiple possible reconnection events; again, its ultimate fate is not stated. Whereas in the latter works the ejecta is transitory, the ejecta of Howison *et al.* (2005) persists for all time.

Here we report our experimental observations of the ejecta sheet's dynamics following normal impact of a spherical drop with a layer of the same liquid. Our visualizations were obtained using high-speed photography with visible light and X-rays. The X-ray technique allows us to see features that in visible light would be obscured by refraction and reflections from free surfaces. We find that the ejecta sheet is always present for Weber numbers above a certain threshold. At low Reynolds numbers the lamella and ejecta form a single contiguous jet, and thus the ejecta persists indefinitely even though at later times it is subsumed into the growing blob on the leading edge of the jet (Keller, King & Ting 1995). At high Reynolds and Weber numbers the ejecta disintegrates. We measured the emergence time, position and speed of the ejecta sheet, and find that these depend strongly on the impact speed and weakly on the viscosity. We show that scaling these quantities with viscosity collapses the data onto master curves that depend only on the impact speed. Lastly, we show that the size of secondary droplets is not necessarily a good indicator of whether the droplets are from the ejecta or the lamella.

2. Experimental system

We conducted experiments to observe the impact of a drop (diameter $D \approx 2$ mm) onto a deep pool of the same fluid (depth > 10 cm) at speeds $U = 1$–5 m s^{-1}. Each drop was formed on the tip of an electrically grounded sewing needle fed by a 30 gauge hypodermic needle connected to a reservoir. The sharp conical tip of the sewing needle minimized surface oscillations and lateral deflections, which greatly reduced variations of the impact location and yielded reproducible drop sizes. The oscillations of the drop after detaching from the needle decayed long before impact, and the small size of the drops ensured that the flattening caused by air drag resulted in a less than 3 % difference between the major and minor axes of the drop. The experimental fluids were a series of silicone oils (Clearco Products) with different viscosities; their physical properties are listed in table 1. Drops were produced at a rate sufficiently slow to allow the waves on the substrate fluid from the preceding drop impact to fully decay.

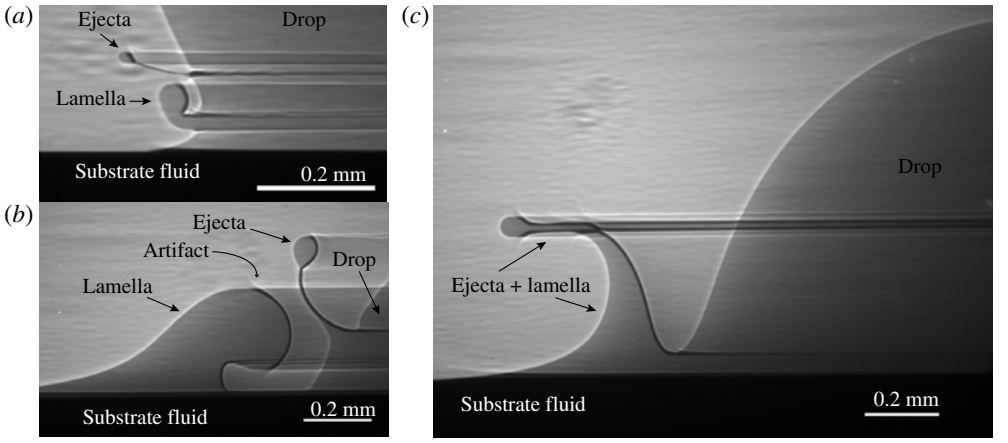

FIGURE 1. X-ray phase contrast images of splash at (*a*) $We = 396$ and $Re = 5703$ with silicone oil (SO1) (*b*) $We = 324$ and $Re = 2191$ with silicone oil (SO3) and (*c*) $We = 451$ and $Re = 710$ with silicone oil (SO6). Panels (*a*) and (*b*) show a thin jet (the ejecta sheet) and a thicker jet (the lamella sheet). Panel (*c*) shows the ejecta and lamella sheet combined into a single contiguous sheet. Note that the leading edge of all jets is engorged due to Taylor–Culick contraction. The wayward halo departing from the lamella in (*b*) is an example of an artifact produced by the phase contrast technique.

	Fluid	Nom. viscosity (cSt)	Viscosity (cP)	Density (g cm^{-3})	Surface tension (dyne cm^{-1})
SO1	Silicone oil	0.65	0.49	0.759	15.7
SO2	Silicone oil	1.00	0.82	0.816	17.2
SO3	Silicone oil	1.50	1.30	0.851	17.6
SO4	Silicone oil	2.00	1.80	0.871	18.6
SO5	Silicone oil	3.00	2.70	0.899	18.4
SO6	Silicone oil	5.00	5.70	0.918	19.4

TABLE 1. Physical properties of experimental fluids.

Our visible light measurements were obtained from a high-speed video camera (Phantom 7.3, Vision Research) or a single lens reflex camera (20D, Canon) in combination with a single 600 ns, 6 J pulse from a spark flash (Palflash 501, Pulse Photonics) triggered by the interruption of a photogate by the drop (see Zhang *et al.* 2010). Our X-ray measurements were conducted at the high-speed imaging facility at the Advanced Photon Source at Argonne National Laboratory using a phase contrast technique (Fezzaa & Wang 2008). The latter technique produces images, such as those shown in figure 1, in which the grey scale is indicative of absorption by the fluid and the fluid–gas interface parallel to the beam is highlighted by a light or dark halo. The substrate fluid appears black in these images because the X-ray beam traverses the full diameter of the container ($\sim$10 cm) and therefore is highly attenuated. The phase contrast technique produces some halo-like artifacts, such as the one indicated in figure 1(*b*), that are easily distinguished by eye or, if necessary, by simulation (see Fezzaa & Wang 2008).

The impact of a drop with a deep layer of the same fluid is conventionally described by six parameters: the impact velocity U, the drop's diameter D or radius R, the fluid's surface tension σ, density ρ and dynamic viscosity η, and the acceleration due to gravity g. These parameters reduce to three dimensionless groupings, which are commonly chosen to be the Weber number $We = \rho DU^2/\sigma$, the Reynolds number $Re = \rho DU/\eta$ and the Froude number $Fr = U^2/gD$. The acceleration due to gravity is assumed to be negligible on the time scale of a splash and henceforth the dependence on the Froude number is ignored.

We measured the kinematic viscosity of our fluid with a Cannon–Fenske routine viscometer, the density with a Gay-Lussac bottle, and the surface tension with the Wilhelmy plate method.

3. Experimental results

3.1. *Phenomenology of the ejecta sheet*

Deegan *et al.* (2008) proposed a classification of splashes in shallow layers in which they differentiated between *crown droplets*, which unambiguously detach from the lamella, and *microdroplets*, whose origin was not determined but which they speculated were produced by the breakup of the ejecta sheet. Thoroddsen *et al.* (2011) recently showed that the ejecta unambiguously produces microdroplets. We examined the initial moments of impact to further characterize the production of the microdroplets. We found that the behaviour at early times, as demonstrated by the examples shown in figure 1, is far more complex than previously thought.

The lamella and ejecta sheets are labelled in figure 1. While figures 1(*a*) and 1(*b*) show two distinct jets, figure 1(*c*) shows a single jet. Furthermore, this single jet is what we would normally classify as a lamella (Zhang *et al.* 2010). We examined the evolution of this jet at all accessible times and find no other jet. This raises the question of whether there is a bifurcation in the dynamics at which the ejecta sheet loses or gains integrity.

We observed splashes over a wide range of *We* and *Re* and found that these follow one of the four behaviours depicted in figure 2: (*a*) the drop merges with the substrate fluid, generating capillary waves as shown by Yarin & Weiss (1995); (*b*) a single jet forms; (*c*) a thin jet (the ejecta) emerges within 100 μs after impact, followed by a thicker one (the lamella), and the ejecta folds into and ultimately merges with the upper part of the drop; and (*d*) like (*c*), two jets are produced but instead the ejecta disintegrates into microdroplets.

Our experiments are summarized in figure 3. For different impact speeds the experiments for a particular fluid trace out a curve $We = \alpha Re^2$. The most revealing experiments are those for SO3 (indicated by an arrow in figure 3), which cross from the *two-jets* to the *one-jet* regime. Experiments with this fluid at moderate and high *We* show two clearly distinct jets. The separation of these jets decreases with *We*. Just above the transition to *one jet*, the jets remain robust and clearly separated, but are very close to each other; just below the transition, there is only a single jet, and furthermore it is shaped as though the ejecta was affixed to the leading edge of the lamella. From these observations we conclude that the ejecta and the lamella merge to form a single jet. Thus, the horizontal segment on the leading edge of the jet visible in figure 1(*c*) is the ejecta riding on the leading edge of the lamella. For all values of *Re* below the transition point the jets remain conjoined.

Thoroddsen *et al.* (2011) provided a different classification of splashes in a parameter range similar to ours. While our data focus exclusively on the

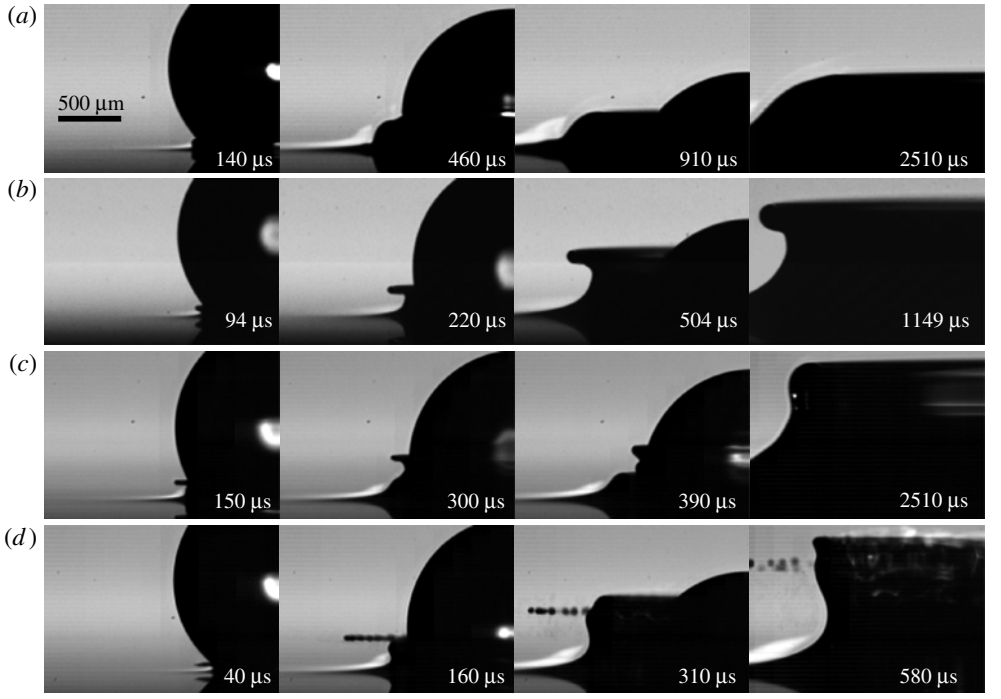

FIGURE 2. Time evolution of jets for: (*a*) $Re = 1330$, $We = 117$; (*b*) $Re = 1511$, $We = 282$; (*c*) $Re = 2931$, $We = 256$; and (*d*) $Re = 4975$, $We = 735$. These parameters are plotted in figure 3 with an open circle, square, star and diamond, respectively. The time after impact is given in the lower right-hand corner of each image, and the scale bar is given in the first panel of (*a*). The black corresponds to the fluid. The various white patches are lighting artifacts.

ejecta dynamics, their categorization focuses on microdroplet production. The two classifications are complementary. For example, their *sling shot* regime falls within our *one-jet* regime, and their *irregular broken sheets and spray* regime corresponds closely to our *two-jets* regime in which the ejecta disintegrates. In the former case, our experiments reveal that the ejecta forms the leading edge of the lamella, whereas their experiments show how this ejecta breaks up. In the latter case, their experiments reveal the presence of microdroplets, whereas our experiments pinpoint their source.

3.2. *Dynamics of the ejecta sheet*

In addition to the morphology, we measured the emergence time, position and speed of the ejecta sheet using high-speed video recording, typically at 50 000 frames s^{-1}. Figures 4(*a*) and 4(*b*) show typical data for the jet position versus time after impact. In order to determine the time when the drop first touches the layer (i.e. $t = 0$), we measured the vertical distance between the bottom pole of the drop and its reflection for several frames prior to impact and extrapolated this value to zero. In all cases we examined, the radial distance of the tip from the centre of the impact r grew rapidly and showed strong signs of deceleration, whereas the vertical position relative to the layer surface z grew slowly and showed weak signs of acceleration.

We determined the speed of the ejecta from the derivative of a fit to the position versus time data, and compared it to the speed of the front u_m that is required to move the mass of fluid from beneath the drop (see Appendix). We define the emergence

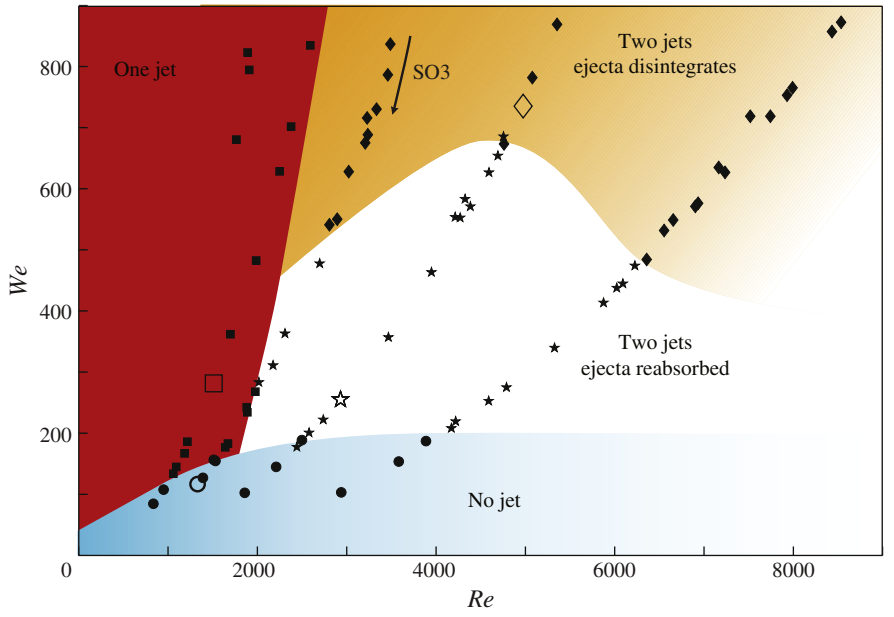

FIGURE 3. (Colour online available at journals.cambridge.org/flm) Phase diagram as a function of *We* and *Re* indicating number of jets resulting from drop impact. The behaviour of each experiment is indicated with a symbol: circles for a non-cresting capillary, squares for a single jet comprising both the ejecta and lamella sheet, stars for separate ejecta and lamella, and diamonds for separate ejecta and lamella when the ejecta dissociates into secondary droplets. Open symbols correspond to the particular experiments depicted in figure 2.

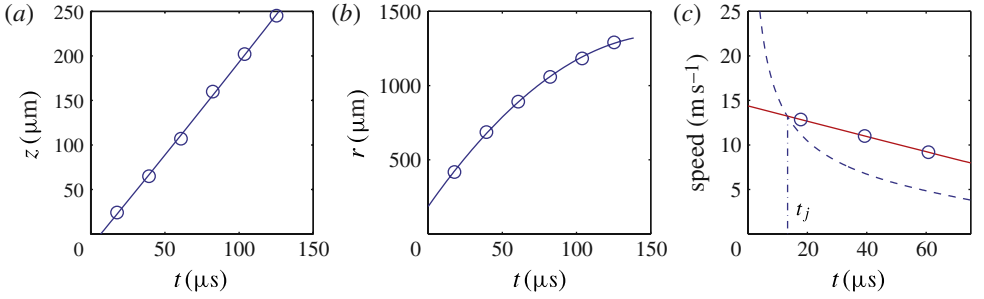

FIGURE 4. (Colour online) Example of the radial r and vertical z position of the ejecta sheet versus time, and the procedure for determining the emergence time t_j. The data for the position of the leading edge plotted versus time after impact (circles) were fitted to a parabola (solid line). The speed of the jet was determined from the derivative of the fit, and plotted in panel (*c*) with a solid (red) line. The speed of the front for the particular impact speed (see Appendix) is plotted with a dashed (blue) line. The intersection of the front and jet speed was taken as the emergence time.

time t_j as the time when these curves intersect, as shown in figure 4(*c*). In all cases, t_j lies in the time interval between the image pair bracketing the visible emergence of the jet. We took the emergence speed u_j and the radial position r_j of the jet as the value of these at t_j.

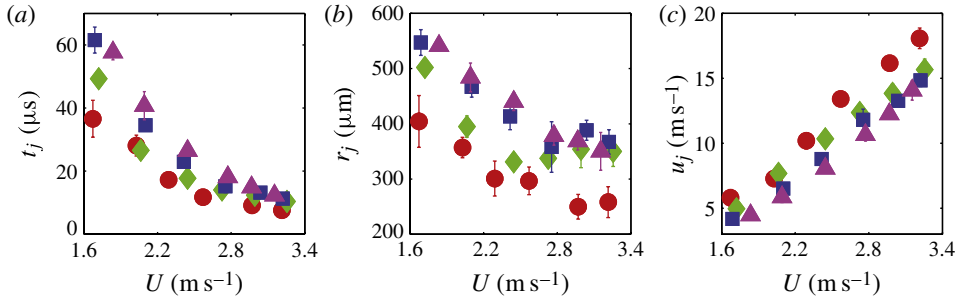

FIGURE 5. (Colour online) The emergence time t_j, radial position r_j and speed u_j of the ejecta sheet plotted versus impact velocity. Symbols correspond to different fluids: circles, SO1 (0.49 cP); diamonds, SO2 (0.82 cP); squares, SO3 (1.3 cP); triangles, SO4 (2.7 cP). The error bars represent the variability of the data for a fixed set of parameters, which is primarily due to the uncertainty in time of first contact between the drop and the layer.

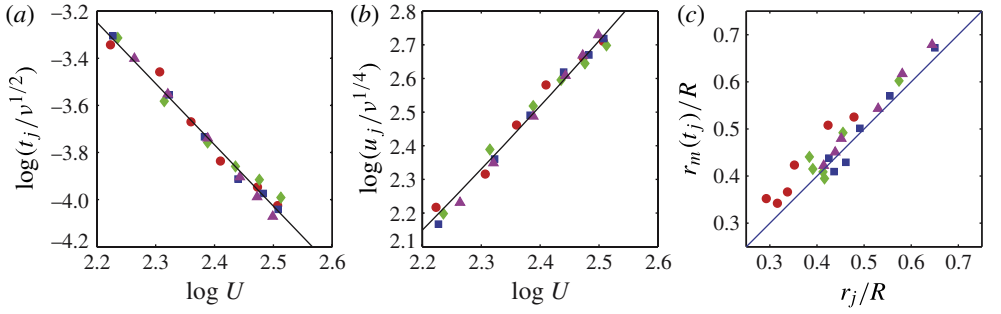

FIGURE 6. (Colour online) (*a*,*b*) Scaled emergence time t_j and speed u_j versus impact speed U plotted on a log–log scale. The solid lines are fits to power laws, which yield exponents of -2.6 and 1.8, respectively. (*c*) Mean radius dictated by mass balance versus the emergence position, both scaled by the radius of the drop. The symbols are the same as in figure 5.

Our measurements for t_j, r_j and u_j are plotted in figure 5 versus impact speed. The most prominent trends are that t_j strongly decreases with impact speed and weakly increases with viscosity, r_j weakly decreases with impact speed and weakly increases with viscosity, and u_j strongly increases with impact speed and weakly decreases with viscosity. The dependence on the impact speed of these quantities is what one would expect qualitatively on the basis of energy conservation. With increasing kinetic energy of the drop, the ejecta ought to be more energetic and thus faster, and a faster jet will outrun the mass front earlier and closer to the origin. The dependence on the viscosity is also what one would expect qualitatively on the basis of energy conservation and the magnitude of jet Reynolds number $Re_j = u_j\delta/\nu$, where δ is the jet thickness. From measurements, $\delta \approx 10$ μm and $Re_j \gtrsim 100$. At these values of Re_j we expect the dissipation to lie between the purely viscous and purely inertial regimes, which would account for the weak dependence on viscosity.

Empirically we find that scaling t_j by $\sqrt{\nu}$ collapses all the experiments to a single curve as shown in figure 6(*a*). Furthermore, that curve is well represented by a power law in the impact speed with an exponent of -2.6.

From this collapse of the emergence time data, it follows that the ejecta speed at emergence will also collapse. By construction $u_j = u_m(t_j)$. For $t \ll R/U$ it follows

that $u_m \sim \sqrt{U/t}$, and thus $u_j \sim \nu^{-1/4}U^{1.8}$. The data shown in figure 6(*b*) verify this scaling. Interestingly, any reasonable and consistent manner of defining u_j produces the same scaling. For example, we tried (i) defining u_j as the earliest measured velocity of the jet, (ii) defining t_j as the moment when the vertical position of the jet is zero (see figure 4) and obtaining u_j by extrapolation, and (iii) choosing $t_j = 0$ and obtaining u_j by extrapolation. In all cases, the scaling of the jet speed is the same, and thus more robust than is apparent from our particular treatment.

Figure 6(*c*) shows the mean radius r_m (see Appendix) versus the emergence radial position. These data show that the jet emerges closer to the centre than the theoretical value of r_m. This is consistent with the inward (i.e. into the fluid) curvature of the meniscus connecting the drop and the fluid layer prior to the emergence of the ejecta. The curvature of the front is expected due to surface tension (see Oguz & Prosperetti 1989). Nonetheless, the rearmost segment of the meniscus lags behind the mean radius, and we observe that it is from this trailing front that the ejecta emerges.

The primary points of comparison for our results are the inviscid simulation of Weiss & Yarin (1999) and Davidson (2002), the experiments of Thoroddsen (2002) and the volume-of-fluid simulations of Coppola, Rocco & de Luca (2011). In our experiments the threshold for the formation of ejecta sheets is a curve in the *Re*–*We* plane, as shown in figure 3. While this curve bends downwards at low *Re*, indicating a significant effect of viscosity, at higher *Re* the dependence on viscosity weakens. Insofar as this trend can be extrapolated to the inviscid limit, our data indicate that the ejecta threshold plateaus to $We \simeq 180$, which is reasonably close to the values predicted by Weiss & Yarin (1999) ($We \simeq 40$) and Davidson (2002) ($We \simeq 200$).

Our results for r_j, t_j and u_j differ in magnitude significantly from those of Thoroddsen (2002) and Coppola *et al.* (2011), but show qualitatively similar trends. We do not expect numerical agreement given the large difference in *We* between our respective experiments: $We = 200$–800 in our experiments, $We = 8000$ in Coppola *et al.* (2011) and $We = 2350$ in Thoroddsen (2002). Nonetheless, we expected the same scaling behaviour. This was not the case either. We find $t_j \sim \sqrt{\nu}/U^{2.6}$, while Coppola *et al.* (2011) find that their data do not follow a (single) power law. We find that $u_j \sim \nu^{-1/4}U^{1.8}$, while Coppola *et al.* (2011) found that $u_j \sim \nu^{-1/2}U^{1.5}$ in agreement with the viscous scaling $u_j \sim \nu^{-1/2}$ found by Thoroddsen (2002). Given that the simulations of Coppola *et al.* (2011) are for the impact of a cylindrical drop, these differences may be due entirely to geometry.

3.3. *Secondary droplets*

As summarized in figure 3, when $We \gtrsim 500$ the ejecta disintegrates and produces a spray of secondary droplets. These droplets are much smaller ($\approx$15 μm) than the typical droplets formed by a crown splash (250 μm; Zhang *et al.* 2010). The presence of a blob on the leading edge of the ejecta (see figure 1) is reminiscent of the engorgement of the lamella's leading edge that precedes its breakup due to a capillary instability (Zhang *et al.* 2010). Moreover, for the particular range of *We* and *Re* studied in Zhang *et al.* (2010), the ejecta and lamella form a single jet and it is the contraction of the ejecta segment of this jet that forms the toroidal blob of fluid that ultimately breaks up. While these similarities suggest that the ejecta disintegrates via a capillary instability, owing to the speed and short life of the ejecta we were unable to explore this possibility.

The small size of the secondary droplets produced by the ejecta partially support the speculation by Deegan *et al.* (2008) that the dichotomy in the size distribution of secondary droplets is due to different jets. Their hypothesis was that *microdroplets*

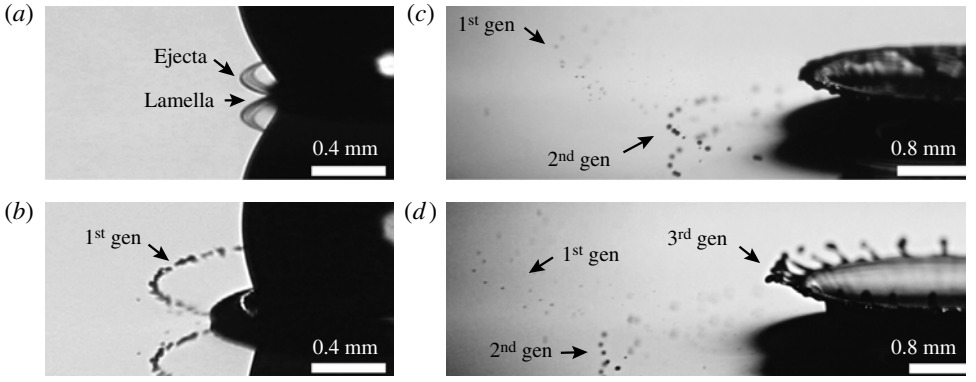

FIGURE 7. Multiple generations of microdroplets emitted from a single impact event for silicone oil (SO1) at $We = 798$ and $Re = 8019$ in a reduced pressure environment (0.17 atm) at 60, 100, 500 and 700 μs after impact with earliest time at top left.

could be attributed to the disintegration of ejecta sheet, while *crown droplets* could be attributed to the breakup of the lamella. While this does occur, as shown by Thoroddsen *et al.* (2011) and in figure 2(*c*), more complicated scenarios are also possible. Figure 7 shows a single impact event that produces three generations of microdroplets, only one of which is due to the breakup of the ejecta sheet; the other generations come from the lamella in separate breakup events. Interestingly, the clear distinction between generations is obscured at full atmospheric pressure. Thoroddsen *et al.* (2011) observed similar dependence on the surrounding gas pressure.

4. Conclusions

The ejecta and the lamella are not sharply distinguished in the literature. One of the principal results of our study is that it provides definitive evidence (see figure 1) that there are two distinct jets. Following the nomenclature established by Weiss & Yarin (1999), there is an ejecta sheet, a high-speed jet formed almost immediately upon impact (within 100 μs), and a lamella sheet, a slower jet that emerges later (typically 500–1000 μs after impact). Our second principal result is that for low *Re* the ejecta and lamella form a single continuous structure. Thus, the seeming absence of an ejecta is now revealed as the case where the ejecta becomes the leading edge of a jet made up of the ejecta and the lamella.

Our measurements of the position, speed and time of the ejecta when it emerges from the neck show that these quantities scale as power laws in the impact speed and the viscosity. Our results are significantly different from previously reported results at similar *Re* but higher *We*. The difference may be indicative of qualitatively different dynamics at higher *We* or of a strong dependence on *We* to which our experiments are insensitive because σ/ρ is almost constant across our series of liquids and thus the variation of *We* is small.

The breakup of the ejecta sheet produces secondary droplets that are much smaller than those typically formed from the lamella. Nonetheless, we observe a typical case in which the secondary drops from the lamella are almost equal in size to those from the ejecta, and thus the size of secondary droplets is not necessarily a good indicator of their origin.

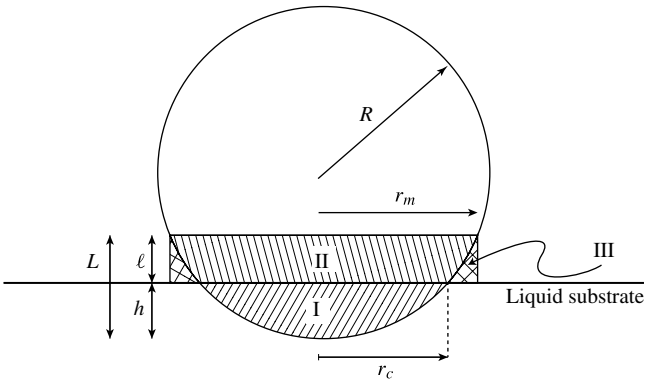

FIGURE 8. Graphic illustrating the geometry of a sphere crossing a plane. When a drop collides with a liquid surface, the volume in region I is displaced. Provided the liquid substrate remains equal to or above its initial flat configuration, which it does in our experiments, the minimum radius that can contain this volume is r_m. We call the edge of domain III the *front*.

Use of the Advanced Photon Source, an Office of Science User Facility operated for the US Department of Energy (DOE) Office of Science by Argonne National Laboratory, was supported by the US DOE under Contract No. DE-AC02-06CH11357. RDD acknowledges support from the James S. McDonnell Foundation 21st Century Science Initiative in Studying Complex Systems – Research Award.

Appendix

As the drop penetrates the liquid substrate, the volume that lies below the substrate level must be displaced radially. We compute the mean radius r_m that contains this displaced volume. Referring to figure 8, the volume below the liquid substrate's surface V_I must be contained in the annular volume V_{III}. Therefore, $V_I = V_{III}$. Furthermore, by geometry $V_{III} = \pi r_L^2(L - h) - V_{II}$, $V_{II} = V_{cap}(R, L) - V_I$ and $V_I = V_{cap}(R, h)$, where $V_{cap}(r, x)$ is the volume of a spherical cap of height x from a sphere of radius r: $(1/3)\pi x^2(3r - x)$. Solving for L yields

$$L = \frac{3}{4}(R + h)\left\{1 - \sqrt{1 - \frac{16}{3}\frac{Rh}{(R + h)^2}}\right\} \tag{A 1}$$

from which $r_m = \sqrt{2RL - L^2}$ can be computed.

For our experiments, $h = Ut$. To leading order at small times $t \ll R/U$: $L \simeq 2Ut$, $r_m \simeq 2\sqrt{URt}$ and $u_m = \mathrm{d}r_m/\mathrm{d}t \simeq \sqrt{UR/t}$. For reference, the geometrical contact point between the drop and the liquid substrate $r_c \simeq \sqrt{2}\sqrt{URt}$. Similar expressions were derived by Oguz & Prosperetti (1989).

REFERENCES

BUTTERWORTH, J. & MCCARTNEY, H. A. 1991 The dispersal of bacteria from leaf surfaces by water splash. *J. Appl. Bacteriol.* **71** (6), 484–496.

COPPOLA, G., ROCCO, G. & DE LUCA, L. 2011 Insights on the impact of a plane drop on a thin liquid film. *Phys. Fluids* **23** (2), 022105.

COSSALI, G. E., MARENGO, M., COGHE, A. & ZHDANOV, S. 2004 The role of time in single drop splash on thin film. *Exp. Fluids* **36** (6), 888–900.

DAVIDSON, M. R. 2002 Spreading of an inviscid drop impacting on a liquid film. *Chem. Engng Sci.* **57** (17), 3639–3647.

DEEGAN, R. D., BRUNET, P. & EGGERS, J. 2008 Complexities of splashing. *Nonlinearity* **21** (1), C1–C11.

FEZZAA, K. & WANG, Y. J. 2008 Ultrafast X-ray phase-contrast imaging of the initial coalescence phase of two water droplets. *Phys. Rev. Lett.* **100** (10), 104501.

HOWISON, S. D., OCKENDON, J. R., OLIVER, J. M., PURVIS, R. & SMITH, F. T. 2005 Droplet impact on a thin fluid layer. *J. Fluid Mech.* **542**, 1–23.

KELLER, J. B., KING, A. & TING, L. 1995 Blob formation. *Phys. Fluids* **7** (1), 226–228.

OGUZ, H. N. & PROSPERETTI, A. 1989 Surface-tension effects in the contact of liquid surfaces. *J. Fluid Mech.* **203**, 149–171.

PASANDIDEH-FARD, M., AZIZ, S. D., CHANDRA, S. & MOSTAGHIMI, J. 2001 Cooling effectiveness of a water drop impinging on a hot surface. *Intl J. Heat Transfer Fluid Flow* **22** (2), 201–210.

REIN, M. 1993 Phenomena of liquid drop impact on solid and liquid surfaces. *Fluid Dyn. Res.* **12** (2), 61–93.

REITZ, R. D. & RUTLAND, C. J. 1995 Development and testing of diesel-engine cfd models. *Prog. Energy Combust. Sci.* **21** (2), 173–196.

RIOBOO, R., BAUTHIER, C., CONTI, J., VOUE, M. & DE CONINCK, J. 2003 Experimental investigation of splash and crown formation during single drop impact on wetted surfaces. *Exp. Fluids* **35** (6), 648–652.

RIOBOO, R., MARENGO, M. & TROPEA, C. 2002 Time evolution of liquid drop impact onto solid, dry surfaces. *Exp. Fluids* **33** (1), 112–124.

SPILLMAN, J. J. 1984 Spray impaction, retention and adhesion – an introduction to basic characteristics. *Pesticide Sci.* **15** (2), 97–106.

THORODDSEN, S. T. 2002 The ejecta sheet generated by the impact of a drop. *J. Fluid Mech.* **451**, 373–381.

THORODDSEN, S. T., THORAVAL, M. J., TAKEHARA, K. & ETOH, T. G. 2011 Droplet splashing by a slingshot mechanism. *Phys. Rev. Lett.* **106** (3), 034501.

WANNINKHOF, R., ASHER, W. E., HO, D. T., SWEENEY, C. & MCGILLIS, W. R. 2009 Advances in quantifying air–sea gas exchange and environmental forcing. *Annu. Rev. Marine Sci.* **1**, 213–244.

WEISS, D. A. & YARIN, A. L. 1999 Single drop impact onto liquid films: neck distortion, jetting, tiny bubble entrainment, and crown formation. *J. Fluid Mech.* **385**, 229–254.

WORTHINGTON, A. M. 1882 On impact with a liquid surface. *Proc. Phys. Soc. Lond.* **34**, 217–230.

YARIN, A. L. 2006 Drop impact dynamics: splashing, spreading, receding, bouncing. *Annu. Rev. Fluid Mech.* **38**, 159–192.

YARIN, A. L. & WEISS, D. A. 1995 Impact of drops on solid surfaces – self-similar capillary waves, and splashing as a new type of kinematic discontinuity. *J. Fluid Mech.* **283**, 141–173.

ZHANG, L. V., BRUNET, P., EGGERS, J. & DEEGAN, R. D. 2010 Wavelength selection in the crown splash. *Phys. Fluids* **22** (12), 122105.